Applied Catalysis B: Environmental 95 (2010) 238–244

Contents lists available at ScienceDirect

Applied Catalysis B: Environmental

journal homepage: www.elsevier.com/locate/apcatb

N- and/or W-(co)doped TiO_2-anatase catalysts: Effect of the calcination treatment on photoactivity

Anna Kubacka [a,*], Gerardo Colón [b], Marcos Fernández-García [a]

[a] Instituto de Catálisis y Petroleoquímica, CSIC, C/Marie Curie 2, 28049 Madrid, Spain
[b] Instituto de Ciencia de Materiales de Sevilla, Centro Mixto CSIC-Universidad de Sevilla, C/Américo Vespucio 49, 41092 Sevilla, Spain

ARTICLE INFO

Article history:
Received 10 November 2009
Received in revised form 16 December 2009
Accepted 22 December 2009
Available online 11 January 2010

Keywords:
Photocatalysis
Titania
Doping
Nitrogen
Tungsten
Nanostructured mixed oxide
Visible and sunlight absorption
Selective partial oxidation
Toluene
Styrene

ABSTRACT

A series of nanosized W,N-codoped and single-doped N- and W-anatase-TiO_2 catalysts have been prepared by a microemulsion method and calcined at different temperatures. The activity in the sunlight selective photo-oxidation of toluene and styrene has been correlated with structural, electronic, and surface examinations of the catalysts done with the help of XRD-Rietveld, N_2 physisorption, X-ray photoelectron, infrared, electron paramagnetic resonance (EPR) and UV–vis spectroscopies. Irrespective of the reaction, W,N-codoped nanocatalysts showed an enhanced photoactivity with respect to bare anatase and single-doped N-TiO_2 and W-TiO_2 materials. A strong W–N synergistic interaction appears to play a decisive role in driving the excellent photoactivity performance of W,N-codoped materials by affecting (i) electronic properties, particularly maximizing the anatase band gap decrease and enhancing the subsequent visible light photon absorption, and (ii) surface properties, in turn related to the formation of OH radicals upon light excitation. The maximum photoactivity is reached by calcination at 450 °C and is concomitantly observed with a near complete selectivity to partial oxidation products. Higher calcination temperatures yielded solids with significantly inferior photocatalytic performance. The properties of the W–N interaction are discussed as a function of the calcination temperature.

1. Introduction

Since the discovery of TiO_2 properties through irradiation [1], heterogeneous photocatalysis has been frequently employed to degradate organic and inorganic pollutants in water and/or air [2–4]. Photocatalytic selective reactions for synthetic purposes are not as common as degradation ones but correspond to a research topic of intense activity in recent years [5–10].

Within the field of photocatalytic synthetic reactions, a particularly interesting reaction scheme would transform aromatic hydrocarbon molecules into high value products of use in chemical/polymer industries through selective oxidation reactions [5,6]. Typical useful catalysts for such reaction mainly concern isolated Ti species on inorganic oxide/zeolitic matrixes but, unfortunately, only allow the use of ultraviolet (UV) sources as excitation energy [5–7,11–13]. We however showed recently that W,N-codoped anatase-TiO_2 nanocatalysts correspond to highly active materials in the gas-phase selective partial oxidation of toluene and styrene upon sunlight excitation [14,15]. After an analysis of the cation–anion combination and the total doping level, we showed that the system with a moderate to high doping level (ca. 10/0.5 at.% of W/N) appears as an efficient photocatalyst displaying both a high reaction rate when compared with P25 and nano-TiO_2, N-TiO_2 or W-TiO_2 reference systems and a near complete selective to partial oxidation products. The synergistic action between the cation and anion doping species in the photochemical activity is grounded in a combined influence on both the structural and electronic properties of the photoactive anatase phase.

In this contribution we attempt to analyze the development of such mutual anion–cation interaction as a function of the calcination temperature in a W,N-codoped catalysts which appear to maintain homogeneity to a reasonable degree in the calcination temperature range going from ca. 400 °C, the lowest temperature where anatase materials coming from sol–gel/microemulsion preparation methods are fully crystallized (e.g. absence of amorphous phases), to ca. 600–650 °C, temperature above which rutile formation from anatase is likely to be initiated [16–18]. To help in understanding the effect of the calcination temperature in W,N-codoped systems we will also undertake the same study in the parent, single-doped N-TiO_2 and W-TiO_2 systems. A different effect of the calcination temperature is expected in anion (N) and cation (W) doping as in the first case we use NH_3 gas as the source of the agent

* Corresponding author. Tel.: +34 91 585 4939/4775; fax: +34 91 585 4760.
E-mail addresses: a.kubacka@icp.csic.es, ak@icp.csic.es (A. Kubacka).

0926-3373/$ – see front matter © 2010 Elsevier B.V. All rights reserved.
doi:10.1016/j.apcatb.2009.12.028

while W is obviously introduced using a microemulsion method and a precursor salt (see Section 2 for details). In spite of this, throughout a multitechnique approach allowing a structural and electronic screening of the (co)doped solids we attempt to provide evidence about the influence of the calcination treatment on the photocatalytic properties of anion and/or cation doped anatase materials. The study interprets (*vide supra*) the different physico-chemical effects triggered by the calcination temperature in our co- and single-doped nanocatalysts and the subsequent differences originated in photochemical activity.

2. Experimental

2.1. Catalyst preparation

Materials were prepared using a microemulsion preparation method by addition of titanium tetraisopropoxide to an inverse emulsion containing an aqueous solution (0.5 M) of ammonium tungsten oxide (Aldrich) dispersed in *n*-heptane, using Triton X-100 (Aldrich) as surfactant and hexanol as cosurfactant. Water/surfactant and water/titanium molar ratios were, respectively, 18 and 110 for all samples [19,20]. The resulting mixture was stirred for 24 h, centrifuged, decanted, rinsed with methanol and dried at 20 °C for 12 h. Following the microemulsion preparation method, the W,N-containing solid precursor was subjected to a heating ramp in 8 (v/v, %) NH_3/N_2 up to 450/600 °C and treated at this temperature in 20 (v/v, %) O_2/N_2 for 2 h. Reference systems concerning single-doped N and W species were synthesized from the corresponding precursors and subjected to the thermal treatment already described expect in the case of single W-containing samples where a 20 (v/v, %) O_2/N_2 gas environment was used throughout the whole treatment. Samples and references nomenclature are detailed in Table 1.

2.2. Photocatalytic experimental details

Gas-phase photodegradation tests were carried out with two organic pollutants (toluene and styrene) and using a set-up described in detail elsewhere [19,21]. As detailed in these sources, activity and selectivity for the gas-phase photo-oxidations were tested in a continuous flow annular photoreactor containing ca. 30 mg of photocatalyst as a thin layer coating on a pyrex tube. The corresponding amount of catalyst was suspended in 1 ml of water, painted on a pyrex tube (cut-off at ca. 290 nm) and dried at RT. The reacting mixture (100 ml/min) was prepared by injecting toluene/styrene (Panreac, spectroscopic grade) into a wet (ca. 75% relative humidity, RH) 20 vol.% O_2/N_2 flow before entering at room temperature to the photoreactor, yielding an organic inlet concentration of ca. 700 ppmv. Under such conditions, the reaction rate shows a zero order kinetics with respect to the total flow and organic pollutant/oxygen concentrations. After flowing the mixture for 6 h (control test) in the dark, the catalyst was irradiated by four fluorescent daylight lamps (6 W, Sylvania F6W/D) with a radiation spectrum simulating sunlight (UV content of 3%; main emission lines at 410, 440, 540, and 580 nm), symmetrically positioned outside the photoreactor. Similar tests were carried out in selected samples using UV lamps (Sylvania F6WBLT-65; 6W, maximum at ca. 360 nm). Reaction rates were evaluated (vide supra) under steady state conditions, typically achieved after ca. 6–10 h (depending on the reaction) from the irradiation starting. No change in activity was detected for all samples within the next 48 h. The concentration of reactants and products was analyzed using an on-line gas chromatograph (Agilent GC 6890) equipped with HP-PLOT-Q/HP-Innowax columns (0.5/0.32 mm I.D. × 30 m) and TCD (for CO_2 measurement)/FID (organic measurement) detectors.

Table 1
Main physico-chemical parameters of the samples.

Sample	W at.% (ICP-AAS/XPS)	N at.% (ICP-AAS/XPS)	S_{BET} ($m^2 g^{-1}$)	Size[a] (nm)
P25	–	–	47	20
Ti	–	–	105	10.4
TiN450	–	0.1/0.5	160	7.6
TiN600		0.2/0.4	119	8.1
WTi450	10.1/10.0		143	7.2
WTi600	10.1/16.6		82	9.9
WTiN450	10.4/9.8	0.3 / 1.5	156	5.7
WTiN600	10.4/13.0	0.8 / 4.9	132	5.9

[a] Obtained for the anatase structure using Scherrer equation.

2.3. Characterization details

Ti:M composition was analyzed by using inductively coupled plasma and atomic absorption (ICP-AAS), while BET surface areas were measured by nitrogen physisorption (Micromeritics ASAP 2010). XRD patterns were recorded in the range $10^\circ < 2\theta < 120^\circ$ using 0.02° steps. X-ray diffraction (XRD) patterns were obtained using a Siemens D-501 diffractometer with Ni filter and graphite monochromator with a Cu K_α X-ray source. DRIFTS spectra were acquired with a Bruker Equinox FT55 equipped with an MCT detector cooled with liquid N_2. UV–vis diffuse reflectance spectroscopy experiments were performed with a Shimadzu UV2100 apparatus with a nominal resolution of ca. 1 nm using $BaSO_4$ as reference.

XPS experiments were performed in a standard UHV chamber (base pressure 3×10^{-9} Torr) equipped with a 100 mm hemispherical electron analyzer (Scienta, SES 100). Mg K_α radiation ($h\nu$ = 1253.6 eV) was used to acquire the core level spectra (O 1s, N 1s, Ti 2p and W 4d). The powder samples were smeared on a carbon tape and the binding energy is referenced to the C 1s peak at 284.6 eV from the carbon tape.

The EPR measurements were done with a Bruker ER200D spectrometer operating in the X-band and calibrated with a DPPH standard. For the 5,5-dimethyl-1-pyrroline N-oxide (DMPO) spin trapping EPR experiments, the samples were suspended in water (at a concentration of 1 g l^{-1}) and were sonicated for 4 min, giving stable suspensions for several hours. An aqueous solution (0.01 M) of DMPO spin trap (supplied by Sigma) was prepared and kept on ice during the whole set of experiments. Bidistilled water (Elix-10) was employed for these preparations. 100 μl of the solid suspension and 100 μl of the DMPO solution were mixed into an EPR flat quartz cell under atmospheric air and irradiated at different times, through a filter with a cut-off at ca. 220 nm, with UV-type lamps identical to those employed for the photoactivity tests, being then immediately transferred to the spectrometer cavity for EPR analysis. At dark conditions no signal is observed and a small radical concentration decay (of ca. 5% on average) can be estimated during the time of the experiments (1 h). The latter were obtained at 20 °C at ca. 9.75 GHz microwave frequency, 19.5 mW microwave power, 100 kHz modulation frequency, 2 G modulation amplitude and 2×10^5 spectrometer gain. No significant signal saturation was observed in those conditions. Blank experiments were also performed over mixtures of 100 μl of the DMPO solution and 100 μl of water to check the absence of radical formation in the absence of solid under the employed conditions.

3. Results and discussion

Under the experimental conditions of this study, reaction products observed are CO_2 and benzaldehyde during toluene photo-oxidation and CO_2, benzaldehyde (plus acetaldehyde), and styrene oxide for styrene photo-oxidation. Such reactions products

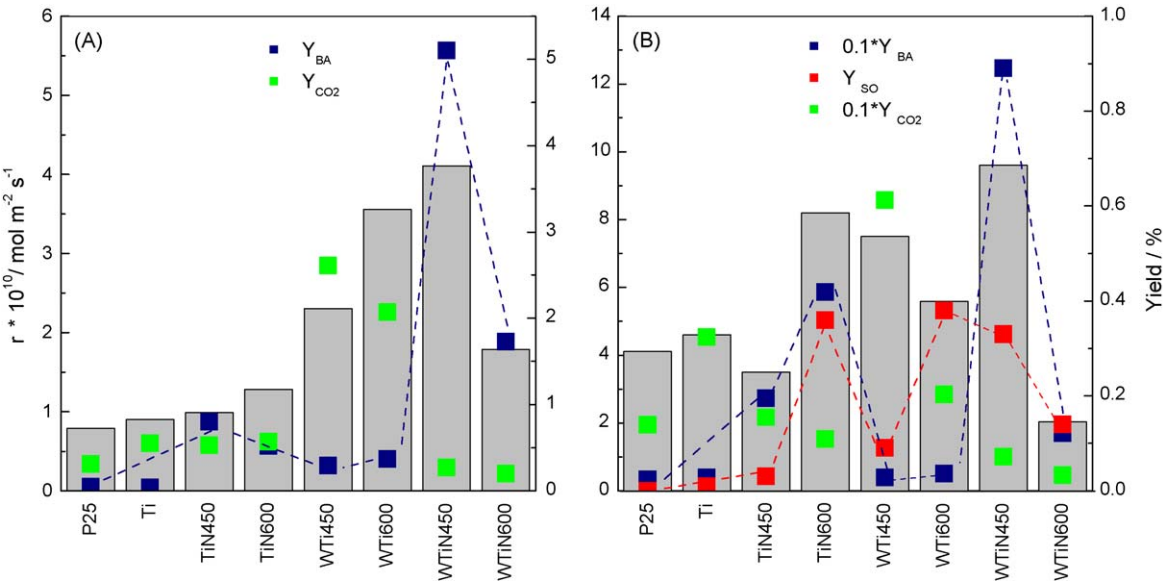

Fig. 1. Experimental results for (A) toluene, and (B) styrene photo-oxidation upon sunlight excitation. Bar: reaction rate (mol m^{-2} s^{-1}); square symbols: yield (%). BA and SO stand for benzaldehyde and styrene oxide, respectively. Lines are guides for the aids.

are the ones expected according to previous results [6,7,14,15,22–24]. Using a high humidity level (as is here the case) likely favors partial oxidation products, allows stable operation over prolonged time periods and, in some cases (e.g. toluene), limits the formation of undesired, noxious reaction products [7,14,15,22–24].

The steady state rates obtained for the single- and codoped samples are summarized in Fig. 1A and B; the higher reaction rates correspond to W,N-codoped systems although some samples, particularly WTi600 for toluene and TiN600 for styrene photo-oxidation, also display significant activity. All single- and codoped samples showed larger activity than titania (P25, nano-TiO_2) references, with maximum reaction rate enhancement of ca 2.5 (styrene) and 4 (toluene) observed for the WTiN450 sample. The comparison of single- and codoped samples shows however than the rate enhancement is significantly inferior when compared with the parent N- or W-containing samples performance; as previously mentioned, samples WTi600/TiN600 displayed a rate only moderately inferior to the more active WTiN450 sample. The calcination temperature affects both single- and codoped samples; its increase seems to favor activity in the case of the N-doping, is clearly negative in the W,N-codoping case, and has a modest and unclear effect (positive for toluene and negative for styrene) in the W-case. Interesting to note, Fig. 2, is the fact that the effect of calcination temperature in W,N-codoped samples when using a UV light excitation source is also negative. This last result together with previous information concerning single-doped materials [19,25] points out the important role played by the visible light. This fact is further discussed below.

The W,N-codoped samples also display important differences with single N- and W-doped catalysts in terms of reaction selectivity. This can be deduced from Fig. 1A and B, which includes information concerning the yield of the reaction products and indicates the pronounced changes in selectivity occurring from single N- and W-doped materials with respect to W,N-codoped nanosolids [14,25]. Partial vs. total (e.g. CO_2) oxidation yield ratio increases by a ca. of an order of magnitude when compared single- and codoped catalysts. The use of W,N-coped anatase-TiO_2 materials has been previously reported for degradation reactions [26,27] but only our previous work showed the usefulness of such type of nanosolids in selective photo-oxidation reactions [14,15]. All W,N-systems studied up to date share however a characteristic

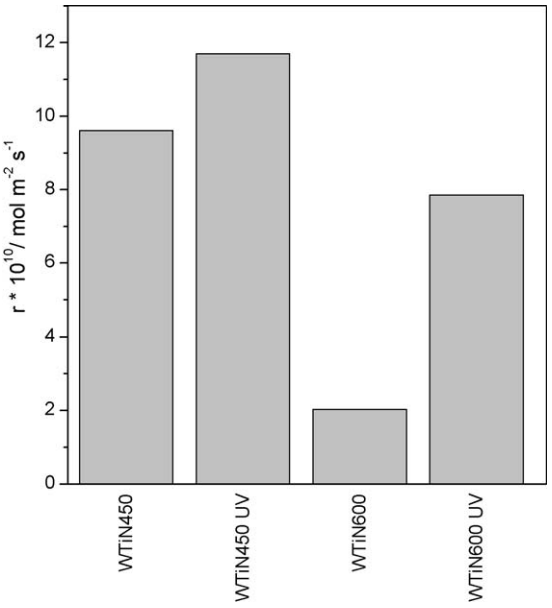

Fig. 2. Reaction rates of W,N-codoped samples for styrene photo-oxidation upon sunlight and UV light (365 nm) excitations.

high activity upon sunlight or visible excitation, although the importance of the UV contribution in the former case seems very different among the different materials tested [14,26]. The calcination temperature appears to have relatively little influence on selectivity except in the single-doped WTi series where some appreciable changes are present in styrene photo-oxidation.

Differences among photocatalytic performance of the samples can be grounded in both structural and electronic factors. Main physico-chemical parameters of the N-, W-, and W,N-doped and titania references are summarized in Table 1. According to XRD patterns (Fig. 3), all samples display a dominant anatase-type structure (JPCDS 84-1286) with potential presence of a residual brookite contribution pointed out by a bump at ca. 32–33°. A lost of crystallinity is nevertheless observed in going from N, to W, and W,N-doped systems. This is also evident from Table 1, surface and

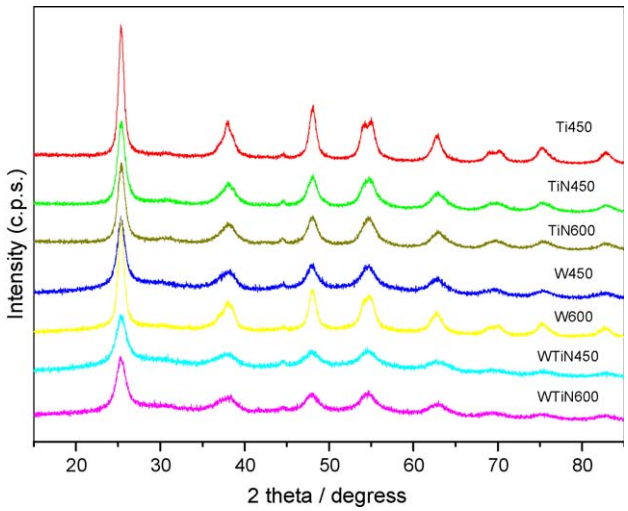

Fig. 3. XRD spectra of the samples.

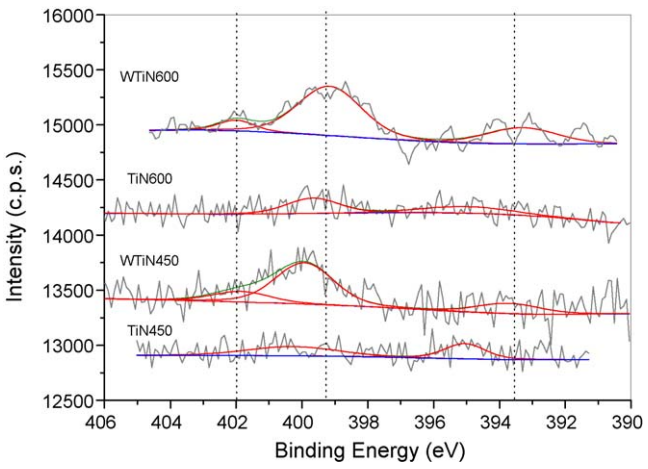

Fig. 4. N 1s XPS peak for N-containing samples.

primary particle size are affected mainly by NH_3 treatment and calcination temperature. As expected, the fist increases surface area and decreases particle size [14,15] while a calcination temperature raising decreases both dispersion and available surface area. In spite of such differences, all samples are high surface area, nanostructured materials with an anatase-type structure.

Differences between single N-, and W-doped and W,N-codoped photocatalytic behavior must be thus grounded in other physico-chemical parameters. To study the chemical state of the doping agents we performed a combined IR/XPS study. Starting with XPS and cations, Table 2 reports the binding energies obtained for the Ti 2p and W 4d levels which are characteristic of Ti(IV) and W(IV) states [28]. Such oxidation states are typical of single W-containing TiO_2 materials [25] although, as stated previously, co-presence of W and N at the anatase structure drives to a Ti2p XPS peak shifted to lower energies [15]. The magnitude of such energy shift seems to depend on N properties as Table 2 showed a similar trend with calcination temperature for single N-doped and W,N-codoped materials. Absence of significant amounts of Ti(III) in the samples was also confirmed with EPR. Changes of XPS binding energies would thus concern Ti and would not imply significant differences for W in single- and codoped samples. An additional, major difference observed by XPS for the Ti/W cations is however related to the W surface concentration in W- and W,N-containing series. As can be seen in Table 1, calcination at 450 °C develops nanocatalysts with a reasonable homogeneity in terms of cation homogeneity throughout the solid while calcination at 600 °C enriches the surface in W. This last fact is more acute in the case of the single-doped WTi series than in W,N-codoped series. Ammonia treatment is therefore stabilizing W into the anatase structure, presumably (as below discussed) by the development of a W–N interaction.

Table 2
XPS Ti 2p and W 4d binding energies (eV) of Ti–W–N samples.

Sample	Ti 2p (eV)	W 4d (eV)
Ti	458.8	–
TiN450	458.9	–
TiN600	458.5	–
WTi450	459.0	247.5
WTi600	459.5	247.7
WTiN450	458.8	247.5
WTiN600	458.5	247.3

The N-content of the samples grows with the calcination treatment temperature for W,N-codoped samples and less markedly for single N-doped materials, and seems to be accumulated at the surface of the solids in all cases (Table 1). N 1s XPS peaks, Fig. 4, are noisy but provide evidence of two well defined contributions at ca. 402.0/399.2 eV and a small contribution at ca. 393.6–393.8 eV for W,N-codoped samples and ca. 395.0 for the N-containing (particularly for TiN450) samples. The ≈393.5 eV peak can be associated to N species at substitutional positions of the anatase structure and strongly affected by the presence of W in the corresponding cases [29–32]. This explains the binding energy difference with respect to similar substitutional N species (≈395.0 eV) detected in the single N-doped catalysts. XPS gives thus a clear fingerprint for a W–N interaction when N is at substitutional positions of the anatase lattice.

The 401.9 and 399.3 eV peaks are ascribed typically to N–H, C–N, or N–O containing surface groups [29–32]. The assignment of N-containing species is easily done with the combined information extracted from a XPS/DRIFT study of the solids [14,33–36]. The FTIR study (Fig. 5) allows to identify $(CN)^{n-}$ (ca. 2230–2235/2210–2217 cm^{-1}; two species) as the major contributors to the high energy XPS peaks [33,35]. The dominance of the 2230–2235 cm^{-1} in W,N-codoped samples may allow to assign this species to the ca. 399.3 eV XPS peak while the other $(CN)^{n-}$ may contribute to the ca. 402 eV peak. It can be also mentioned that other N-containing species may be present and some very minor DRIFTS contributions (3015/2855 cm^{-1}) of $(NH_x)^{n+}$ species are observed (result not shown) and may contribute, as previously postulated, to the higher binding energy XPS peak [29–32]. Although the XPS assignment has certain uncertainty, it is clear that the two $(CN)^{n-}$ are distinctive of the sample nature and, particularly, of the presence/absence of W. This would indicate the close presence of N and W impurities in the case of W,N-codoped materials.

Summing up the structural results obtained in the study we can note that main differences between single- and codoped samples concern, on the first place, the surface amount of W, always lower in the codoped series and particularly significant for samples calcined at 600 °C. The larger quantity of N-containing species in the codoped series and the presence of a small difference on the N-containing species chemical nature concerning both substitutional and CN-type species are noticed as the second main structural difference between single- and codoped materials. The latter is of importance as suggests a close proximity of N and W in the codoped series, with structural influence on both the cation and anion doping ions.

The structural differences between single- and codoped samples had several electronic consequences. UV–vis spectra of

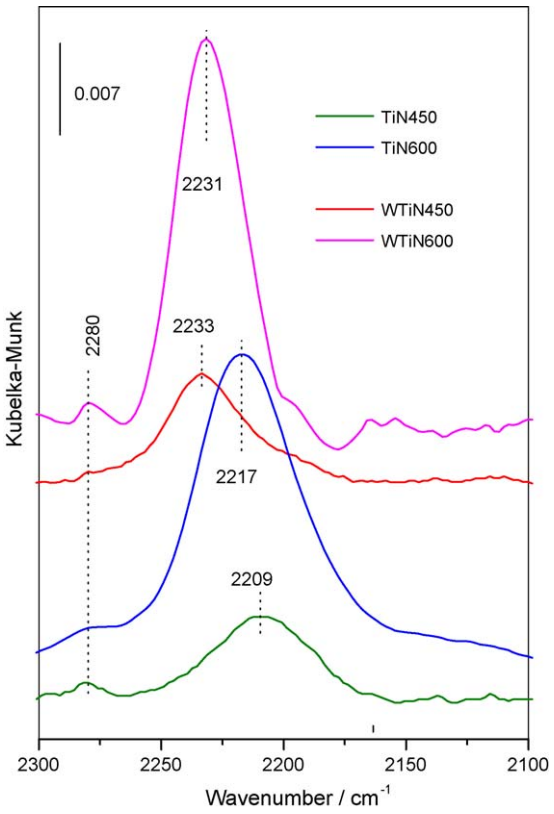

Fig. 5. Background-substrated difference DRIFTS spectra of samples. Difference spectra are obtained by subtracting the W-doped reference signal from the corresponding W,N-codoped spectrum. See text for details.

the single N- and W- and W,N-codoped materials are displayed in Fig. 6. The plot enables investigation of two main physico-chemical features. First, there is an important band gap modification with respect to Ti/TiN/WTi references. Table 3 collects band gap energy values calculated considering anatase an indirect gap semiconductor [34,37]. Only in the case of the WTiN600 samples the spectrum does not allow to obtain an estimation of the band gap energy. For calcination at 450 °C, the combination of N and W seems to produce an additional effect to the one triggered by the presence of W-alone [25], consisting on the additive decrease of ca. 0.2–0.3 eV. This gives a significant (ca. 0.5–0.6 eV) band gap decrease for the W,N-codoped samples with respect to bare

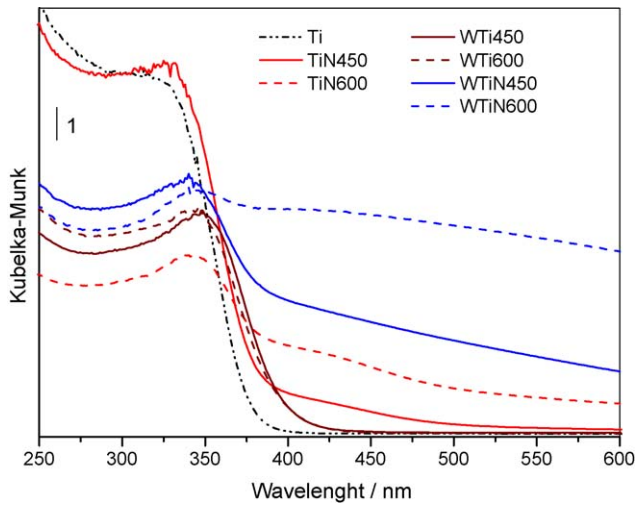

Fig. 6. UV–vis spectra of the W–Ti–N samples.

Table 3
UV–vis main features of W,N-codoped and reference samples.

Sample	Band gap (eV)	Gap features (nm)
Ti	3.1	–
TiN450	3.0	410–500
TiN600	2.65	410–500
WTi450	2.9	–
WTi600	2.95	
WTiN450	2.55	480–650
WTiN600	–	480–750

anatase or titania (P25, Ti) references. At 600 °C we observed also a change on band gap energy for the single N-containing sample, which may indicate a modification of the valence band structure [38]. This is however difficult to be accepted without doubt due to both the additional presence of localized states (Fig. 6) and the limited amount of N present in the material (Table 1) [34]. In any case, the small changes for single W-doped samples (in fact, the red shift detected in the gap is lower than at 450 °C, a fact clearly connected with the exclusion of W from the anatase structure) and the impossibility to measure such changes for WTiN600 makes limit the analysis at the high calcination temperature.

The presence of N additionally affects optical properties of the samples in the visible range. Table 3 summarizes the energy region where broad features are detected. A comparison with the TiN reference indicates a more dramatic effect of the dopant anion in the presence of W. While single N-containing samples display the typical shoulder center at ca. 430–460 nm associated to localized electronic states near the conduction band [14,34–36], W,N-codoped samples display a continuous bump from the anatase gap to ca. 650–750 nm. It is obvious that this broad-energy feature reflects the heterogeneity of N (more strictly speaking W–N) impurities and associated charge-neutrality defects present on the samples.

The effects on band gap seem to be directly related to the photocatalytic performance of W,N-codoped materials with respect to single N- and W-containing samples. The larger the red shift of the gap, the higher the activity. The negative effect of the calcination temperature observed for the W,N-codoped series may be associated to a combined effect of W exclusion from the anatase structure together with the larger heterogeneity of the N-containing species (more precisely, as previously demonstrated by the structural analysis of the W–N and charge-compensation defect structures) some of which may be detrimental for activity. Presence of W surface patches has been shown detrimental for photoactivity in the single W-doped parent materials [25]. Although no clear answer can be here obtained concerning the role of W–N entities, Fig. 2 points out that most of the negative effects concern visible and not UV light photons. Together with result of Fig. 1 would suggest that the negative effect of the calcination temperature raising above 450 °C in W,N-codoped samples can be ascribed to a complex W–N-defect related electronic states with no direct correspondence in either single N- or W-doped nanocatalysts. This additionally suggests that certain localized gap states active in capturing visible light photons may be detrimental for activity.

Surface differences among samples may be of importance to interpret activity; however, our previous measurements of surface acidity showed no apparent correlation with photoactivity in W,N-codoped catalysts [14,15]. As in our experimental conditions hydrocarbon photo-oxidation mainly proceed trough a mechanism involving OH radicals [22–24], Fig. 7 attempts a new approach to investigate surface properties upon illumination and summarizes results of a EPR study of OH radicals using DMPO as a spin trapping molecule. Sunlight irradiation of DMPO-containing sample suspensions gives rise to a signal with 1:2:2:1 intensity pattern for all

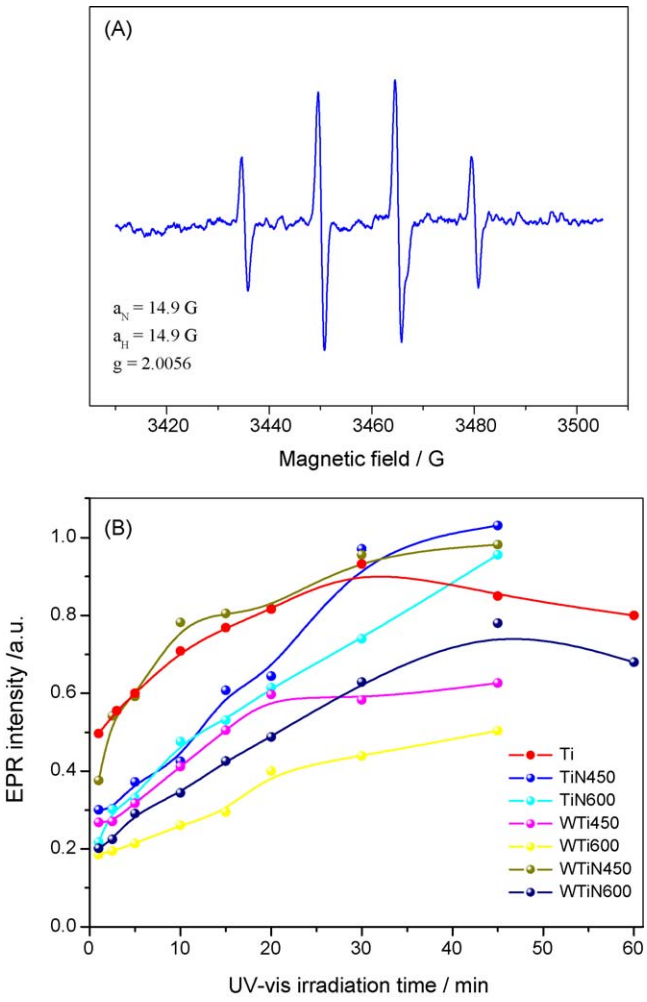

Fig. 7. (A) Representative EPR spectra of DMPO-sample aqueous suspension after 10 min UV light irradiation. (B) Evolution of the DMPO-OH signal intensity for samples as a function of irradiation time.

samples (Fig. 7A). Its EPR parameters (g = 2.0056, a_N = 14.9 G, a_H = 14.9 G) are characteristic of DMPO-OH adducts [39–42]. The intensity of the DMPO-OH adduct signal as a function of the time under UV irradiation is plotted in Fig. 7B. The WTiN450 sample displays a continuous growing behavior with a quick raising start followed by a smooth increase up to the end of the experiment. The remaining samples, on the contrary, showed rather smooth initial step which develops up to significantly larger times. The existence of a second stage on the DMPO-OH adduct signal is likely an effect of multiple additions, within consecutive reactions, of OH radicals to DMPO molecules to yield diamagnetic species [39,42].

Photocatalytic differences among samples as a function of the sample nature and calcination temperature would be linked with differences in hole (e.g. OH) handling properties that the EPR analysis of DMPO-OH signals may help to uncover. Fig. 8 attempts to provide a correlation between the reaction rates observed for toluene and styrene photo-oxidation and the initial rate for OH radical formation as measured by the slope of the initial (linear) region of the intensity plot displayed in Fig. 7B. The rising of the calcination temperature seems to evidence a clear difference between the behavior of the WTi/WTiN series and the TiN one. In the first case, a lower rate in the initial formation of OH radicals is essentially detrimental for activity (with the exception of the WTi series for toluene). This is the result expected if the involvement of the OH radicals, already described for the photo-oxidation of aromatic hydrocarbons [22,24], plays a dominant role, for example,

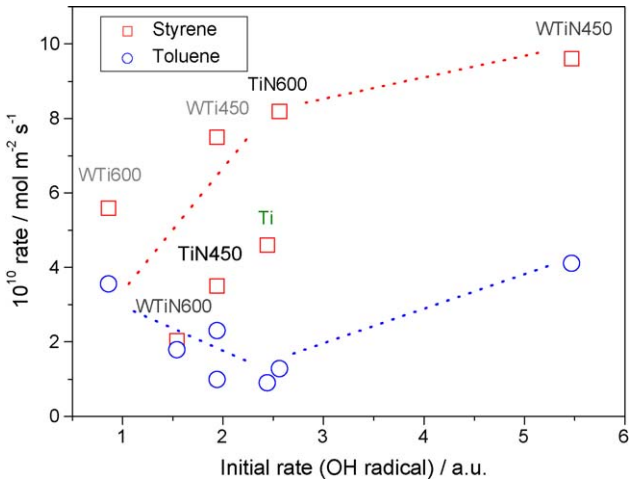

Fig. 8. Correlation plot between the initial rate of OH radical formation and reaction rate for styrene and toluene photo-oxidation. Lines are only guides for the aids.

is related or occurs before the slow step of the reaction rate. However, previous results on W-samples [19] as well as the exception of the TiN series may indicate that this would not be the general case. In fact, the plot indicates the existence of two well defined regions. It seems that a dominant role of the OH radicals may be possible for samples having a significant surface density, this would differentiate sample WTiN450 for the rest of samples, while photoactivity differences among the remaining samples appear a more complex phenomenon, grounded in more complex physico-chemical differences, which need further input to be adequately addressed.

4. Conclusions

The present work has explored the simultaneous W–N doping of the anatase structure and, particularly, the influence of the calcination temperature in the photoactivity of the samples. We synthesized solids by a microemulsion method following with a NH_3 treatment. These materials contain both W and N at substitutional positions of the anatase network but also other N-containing chemical species as $(CN)^{n-}$ species located mainly at bulk positions. Other N-containing species like $(NH_x)^{n+}$ are detected in small quantities and are likely at the surface of the materials. Structural results obtained in the study show that main differences between single- and codoped samples concern, on the first place, the surface amount of W, always lower in the codoped series and particularly significant for samples calcined at 600 °C. The larger quantity of N-containing species in the codoped series and the presence of a small difference on the N-containing species chemical nature, which suggests a close proximity of N and W in the codoped series, correspond to the second main difference between single- and codoped materials.

The W,N-codoping process produces drastic effects on both activity and selectivity of aromatic hydrocarbon photo-oxidation using sunlight. Enhancement factors up to ca. 5 times were obtained on the reaction rates with respect to nano-TiO_2 and P25 reference catalysts. The activity enhancement is also detected for W,N-containing formulations with respect to single N-TiO_2 and W-TiO_2 parent materials and is likely grounded in the lack of W-rich patches/zones and the influence of W–N defect structures in (i) electronic properties, particularly in maximizing the anatase band gap decrease and enhancing the subsequent visible light photon absorption, and (ii) surface properties, in turn related to the formation of OH radicals upon light excitation. The global positive effect is maximized after calcination at 450 °C, calcination

temperatures above that point being detrimental for photocatalytic performance.

Acknowledgements

A.K. thanks the CSIC for a I3P post-doctoral grant. Financial support by the projects CTQ-2007-60480/BQU, and P06-FQM-1406 is fully acknowledged.

References

[1] A. Fujishima, K. Honda, Nature 230 (1972) 37.
[2] M.R. Hoffman, S.T. Martin, W. Choi, D.W. Bahneman, Chem. Rev. 95 (1995) 69.
[3] O. Carp, C.L. Huisan, A. Reller, Prog. Solid State Chem. 32 (2004) 33.
[4] H. Thu, M. Karkmaz, E. Puzenat, C. Guillard, J.M. Herrmann, Res. Chem. Intermediat. 31 (2005) 449.
[5] A. Maldotti, A. Molinari, R. Amadelli, Chem. Rev. 102 (2002) 3811.
[6] Y. Shiraishi, T. Hirai, J. Photochem. Photobiol. C 9 (2008) 157.
[7] X. Li, C. Kutal, J. Mater. Sci. Lett. 21 (2002) 1525.
[8] P. Du, J.A. Moujlin, G. Mul, J. Catal. 238 (2006) 342.
[9] V. Augugliaro, T. Caronna, V. Loddo, G. Marci, G. Palmisano, L. Palmisano, Y. Yurkadal, Chem. Eur. J. 14 (2008) 4640.
[10] S. Yurkadal, G. Palmisano, V. Loddo, V. Augugliaro, L. Palmisano, J. Am. Chem. Soc. 130 (2008) 1568.
[11] M.A. González, S.G. Howell, S.K. Silkar, J. Catal. 183 (1999) 159.
[12] C. Murata, T. Hattori, H. Yoshida, J. Catal. 231 (2005) 292.
[13] Y. Shiraishi, M. Morishita, T. Hirai, J. Phys. Chem. B 110 (2006) 17898.
[14] A. Kubacka, B. Bachiller-Baeza, G. Colón, M. Fernández-García, J. Phys. Chem. C 113 (2009) 8553.
[15] A. Kubacka, B. Bachiller-Baeza, G. Colón, M. Fernández-García, Appl. Catal. B 93 (2010) 274.
[16] M. Fernández-García, X. Wang, C. Belver, J.C. Hanson, J.A. Rodriguez, J. Phys. Chem. C 111 (2007) 674.
[17] M. Fernández-García, X. Wang, C. Belver, J.C. Hanson, J.A. Rodriguez, J. Am. Chem. Soc. 129 (2007) 13604.
[18] A.S. Barnard, H. Xu, ACS Nano 2 (2008) 2237.
[19] A. Fuerte, M.D. Hernández-Alonso, A.J. Maira, A. Martínez-Arias, M. Fernández-García, J.C. Conesa, J. Soria, G. Munuera, J. Catal. 212 (2002) 1.
[20] N. Uskokovic, M. Dofrenik, Surf. Rev. Lett. 12 (2005) 239.
[21] A.J. Maira, K.L. Yeung, J. Soria, J.M. Coronado, C. Belver, C.Y. Lee, V. Augugliaro, Appl. Catal. B 29 (2001) 327.
[22] G. Marcí, M. Addamo, V. Augugliaro, S. Coluccia, V. Loddo, G. Matra, L. Palmisano, M. Schiavello, J. Photochem. Photobiol. A 160 (2003) 105.
[23] T. Guo, Z. Dai, C. Wu, T. Zhu, Appl. Catal. B 79 (2008) 171.
[24] M. Sleiman, P. Conchon, C. Ferronato, J.-M. Chovelon, Appl. Catal. B 86 (2009) 159.
[25] A. Kubacka, M. Fernández-García, G. Colón, J. Catal. 254 (2008) 272.
[26] J. Li, J. Xu, W.-L. Dai, H. Li, K. Fan, Appl. Catal. B 82 (2008) 233.
[27] Y. Shen, T. Xion, T. Li, K.T. Yang, Appl. Catal. B 83 (2008) 177.
[28] C.D. Wagner, W.M. Riggs, L.E. Davis, J.F. Moulder, in: G.E. Muller (Ed.), Handbook of X-Ray Photoemission Spectroscopy, PerkinElmer, Minnesota, 1976.
[29] A.V. Emeline, V.N. Kuznetsov, U.K. Rybakutv, N. Serpone, Int. J. Photoenergy (2008), art. no. 25839.
[30] Y. Zhao, X. Qui, C. Burda, Chem. Mater. 20 (2008) 2629.
[31] E. Finazzi, C. Di Valentin, A. Selloni, G. Pacchioni, J. Phys. Chem. B 111 (2007) 9275.
[32] G. Colón, P. Sampedro, M. Fernández-García, H. Chen, J.C. Hanson, J.A. Rodríguez, Langmuir 24 (2008) 11111.
[33] C. Belver, R. Bellod, S. Steward, F.G. Requejo, M. Fernández-García, Appl. Catal. B 65 (2006) 309.
[34] N. Serpone, J. Phys. Chem. B 110 (2006) 24287.
[35] C. Li, L. Chen, N.M. Dimitriojevic, K.A. Gray, Chem. Phys. Lett. 451 (2008) 75.
[36] S. Livraghi, M.R. Chierotti, E. Giamello, G. Magnacca, M.C. Paganini, G. Cappeletti, C.L. Bianchi, J. Phys. Chem. C 112 (2008) 17244.
[37] M. Fernández-García, A. Martínez-Arias, J.C. Hanson, J.A. Rodríguez, Chem. Rev. 104 (2004) 4063.
[38] R. Asahi, T. Morikawa, T. Ohwaki, K. Aoki, Y. Ega, Science 293 (2001) 269.
[39] M.A. Grela, M.E.J. Coronel, A.J. Colussi, J. Phys. Chem. 100 (1996) 16940.
[40] E.G. Janzen, N. Sankuratry, Y. Kotake, J. Magn. Reson. 111 (1996) 254.
[41] D. Dvoranová, V. Brezová, M. Mazur, M.A. Malati, Appl. Catal. B 37 (2002) 91.
[42] A. Kubacka, M. Ferrer, A. Martínez-Arias, M. Fernández-García, Appl. Catal. B 84 (2008) 87.